Science of the Total Environment 859 (2023) 160210

Contents lists available at ScienceDirect

Science of the Total Environment

journal homepage: www.elsevier.com/locate/scitotenv

Pollution mechanisms and photochemical effects of atmospheric HCHO in a coastal city of southeast China

Taotao Liu [a,b,c], Yiling Lin [a,d], Jinsheng Chen [a,b,*], Gaojie Chen [a,b,c], Chen Yang [a,b,c], Lingling Xu [a,b], Mengren Li [a,b], Xiaolong Fan [a,b], Fuwang Zhang [e], Youwei Hong [a,b,*]

[a] Center for Excellence in Regional Atmospheric Environment, Institute of Urban Environment, Chinese Academy of Sciences, Xiamen, China
[b] Key Lab of Urban Environment and Health, Institute of Urban Environment, Chinese Academy of Sciences, Xiamen, China
[c] University of Chinese Academy of Sciences, Beijing, China
[d] College of Chemical Engineering, Huaqiao University, Xiamen, China
[e] Environmental Monitoring Center of Fujian, Fuzhou, China

HIGHLIGHTS

- HCHO photochemical effects were diagnosed by field observations and models.
- Secondary photochemical formation made the largest contributions to HCHO.
- Strong photochemical conditions constrain high HCHO levels in certain situations.
- HCHO mechanism increased by 36 % and 31 % in ROx and O_3 formation, respectively.

GRAPHICAL ABSTRACT

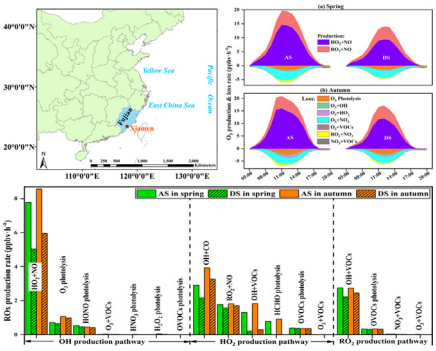

ARTICLE INFO

Editor: Jianmin Chen

Keywords:
HCHO
Formation mechanism
Atmospheric oxidation capacity
Radical chemistry
Photochemical effects

ABSTRACT

Formaldehyde (HCHO) is a vital reactive carbonyl compound, which plays an important role in the photochemical process and atmospheric oxidation capacity. However, the current studies on the quantification of HCHO impacts on atmospheric photochemistry in southeast coastal areas of China with an obvious upward trend of ozone remain scarce and unclear, thus limiting the full understanding of formation mechanism and control strategy of photochemical pollution. Here, systematic field campaigns were conducted at a typical coastal urban site with good air quality to reveal HCHO mechanism and effects on O_3 pollution mechanism during spring and autumn, when photochemical pollution events still frequently appeared. Positive Matrix Factorization model results showed that secondary photochemical formation made the largest contributions to HCHO (69 %) in this study. Based on the photochemical model, the HCHO loss rates in autumn were significantly higher than those in spring ($P < 0.05$), indicating that strong photochemical conditions constrain high HCHO levels in certain situations. HCHO mechanism increased the ROx concentrations by 36 %, and increased net O_3 production rates by 31 %, manifesting that the reduction of HCHO and its precursors' emissions would effectively mitigate O_3 pollution. Therefore, the pollution characteristics and photochemical effects of HCHO provided significant guidance for future photochemical pollution control in relatively clean areas.

* Corresponding authors at: Center for Excellence in Regional Atmospheric Environment, Institute of Urban Environment, Chinese Academy of Sciences, Xiamen, China.
E-mail addresses: jschen@iue.ac.cn (J. Chen), ywhong@iue.ac.cn (Y. Hong).

http://dx.doi.org/10.1016/j.scitotenv.2022.160210
Received 28 August 2022; Received in revised form 10 November 2022; Accepted 12 November 2022
Available online 14 November 2022

1. Introduction

Formaldehyde (HCHO) is an important pollutant of photochemistry, and also is one of the most abundant reactive carbonyl compounds in the troposphere, which plays a critical role in the atmospheric oxidation capacity and radical chemistry (Bao et al., 2022; de Blas et al., 2019; Edwards et al., 2014). Current studies had found that the production rate of HCHO to hydroxyl radical (OH) and hydroperoxyl radical (HO_2) was 1 order of magnitude higher than that of ozone (O_3) (Liu et al., 2022a; Liu et al., 2022b; Zhang et al., 2021a). However, the quantitative analysis of HCHO contribution to photochemical pollution is still the hotspot and difficult topic of current research (Zhang et al., 2021a).

HCHO is directly emitted from anthropogenic activities (such as vehicle exhausts and industrial activities) and natural emissions (such as biomass burning, vegetation, and seawater) (Anderson et al., 2017; Lowe and Schmidt, 1983; Luecken et al., 2018). The secondary formation of HCHO from the photo-oxidation of volatile organic compounds (VOCs) is also a significant source (Anderson et al., 2017; Zeng et al., 2019). The chemical reactions of VOCs with $OH/NO_3/O_3$ can produce HCHO, in which the alkoxy radical reactions ($RO + O_2$) have significant contributions to HCHO formation (Ling et al., 2017; Yang et al., 2020). Photolysis and oxidation with OH radicals are the main loss pathways of HCHO, which can directly produce HO_2 radicals and indirectly produce OH radicals by oxidizing NO to NO_2 (Liu et al., 2015; Zhang et al., 2021a).

With the aggravation of O_3 pollution, the research on HCHO has been widely reported around the world because of its significant impact on photochemical reactions (He et al., 2020; Li et al., 2017b; Li et al., 2014; Nussbaumer et al., 2021; Ou et al., 2016; Villanueva et al., 2021; Yu et al., 2006; Zhu et al., 2017). These studies mainly focused on pollution levels, sources, and identification of the dominant precursors (Cheng et al., 2014; Guo et al., 2009; Li et al., 2010; Ling et al., 2017; Louie et al., 2013; Yang et al., 2017; Yang et al., 2019), and the explorations of HCHO chemical mechanisms and theirs contributions to O_3 pollution were limited. The related studies were concentrated on the megacities and regions with rapid economic development in China, such as Beijing (Liu et al., 2015; Yang et al., 2018) the Yangtze River Delta (YRD) (Li et al., 2018a; Ling et al., 2017), and the Pearl River Delta (PRD) region (Li et al., 2014; Ling et al., 2017). Isoprene was an important precursor of HCHO in regional background, rural, and suburban regions (Li et al., 2014; Yang et al., 2020). In urban sites, alkenes degradation contributed most to HCHO formation (Ling et al., 2017; Liu et al., 2015). A few studies reported that the influence of HCHO photochemical reactions accounted for 9 %–14 % of atmospheric oxidation and 15 % of HO_2 formation, and reducing HCHO led to a decrease of 31 % in O_3 formation (Zeng et al., 2019; Zhang et al., 2021b). Different types and sources for HCHO precursors leading to complicated photochemical reactions mechanisms in other regions should be further studied, except for the characteristics of precursors, the change of meteorological conditions is one of the main factors affecting the concentration, spatial distribution, and formation mechanism of pollutants, furthermore, the meteorological conditions vary from place to place (Liu et al., 2022b; Wang et al., 2018; Wu et al., 2019).

Xiamen is a typical coastal city of Southeast China with relatively low levels of O_3 precursors, which were higher than those in background and remote sites, but lower than those in most urban/suburban areas and even some rural regions (Table S1). However, the city frequently appeared O_3 pollution events in spring and autumn, when the meteorological conditions were governed by synoptic patterns of the quasi-stationary front and the west pacific subtropical high (Liu et al., 2022b; Wu et al., 2019). Moreover, this region is an important transport path between YRD and PRD regions under the control of the East Asian monsoon (Liu et al., 2022b). The favorable photochemical reaction conditions (including high air temperature, intensive solar radiation, and stagnant atmosphere) brought by synoptic patterns provided a good 'laboratory' to further explore HCHO formation mechanism and its impact on O_3 formation. Based on the systematic observations and the application of photochemical model in this study, we aim (1) to reveal the pollution characteristics and source apportionment of HCHO, (2) to clarify the HCHO formation mechanism and sensitivity to precursors, and (3) to quantify the impacts of HCHO on atmospheric oxidation capacity, radical chemistry, and O_3 formation.

2. Methodology

2.1. Site descriptions and field measurement

Xiamen sits on the west coast of the Taiwan Strait. The observations were based on the Atmospheric Environment Observation Supersite (AEOS, 24.61° N, 118.06° E), which was about 70 m above the ground in the Institute of Urban Environment, Chinese Academy of Sciences in Xiamen. The site is a typical urban site, surrounded by highways, shopping malls, educational institutions, administrative, and residential areas. The field campaigns were continuously conducted from May 15 to June 9, 2021, and September 5 to 30, 2021, when typical photochemical pollution occurred frequently under the influence of various synoptic patterns.

HCHO analyzer (FMS-100, Focused Photonics Inc., Hangzhou, China) collected gaseous HCHO by an H_2SO_4 stripping solution and quantified HCHO mixing ratios through detection by fluorescence at $\lambda = 510$ nm (Glowania et al., 2021; Hu et al., 2022). The HCHO liquid solution quantification is based on the Hantzsch reaction, and the stainless steel tube for heating efficiency and the ceramic fiber board thermal insulation layer for thermal insulation efficiency were used to control the reaction temperature of the mixed solution in the reaction chamber to achieve a high signal acquisition frequency in our study. The different dilutions of the HCHO standard solution and a blank were used to make a multi-point calibration every week. The detailed accuracy and repetition rate testing were shown in Table S2. Gas chromatography coupled with a mass spectrometer (GC-FID/MS, TH-300B, Wuhan Tianhong Instruments Co., China) analyzed the VOCs with a 1-hour time resolution. The flame ionization detector (FID) using a PLOT (Al_2O_3/KCl) column (15 m × 0.32 mm × 6.0 μm) measured the hydrocarbons with 2– 5 carbons; a DB-624 column (60 m × 0.25 mm × 1.4 μm) was used to quantify the other VOCs compounds. The instrument system can quantitatively analyze 106 VOCs, including 29 alkanes, 11 alkenes, one alkyne, 17 aromatics, 35 halogenated hydrocarbons, and 13 OVOCs (Table S3). The single-point calibration and multi-point calibration were performed every day and every month with the standard mixtures of PAMS and TO15, respectively.

PAN analyzer (PANs-1000, Focused Photonics Inc., Hangzhou, China) through gas chromatography with electron capture detector (GC-ECD) analyzed PAN, and the single-point calibration and the multi-point calibration were conducted every week and every month, respectively. HONO was monitored by the Monitoring Aerosols and Gases in Ambient Air (MARGA, ADI 2080, Applikon Analytical B.V., the Netherlands). Criteria air pollutants (i.e. O_3, NOx, and CO) were measured by the Thermo Instruments TEI 49i, 42i, and 48i (Thermo Fisher Scientific, Waltham, MA, USA), respectively. The meteorological parameters, such as pressure (P), air temperature (T), relative humidity (RH), wind speed (WS), and wind direction (WD), were offered by a weather station with sonic anemometer (150WX, Airmar, USA). Photolysis frequencies (i.e. JHCHO, JO^1D, JNO_2, JHONO, JH_2O_2, and JNO_3) were monitored by a photolysis spectrometer (PFS-100, Focused Photonics Inc., Hangzhou, China). Table S4 shows the detailed uncertainty, detection limit, and time resolution of instruments for trace gas observation. The AEOS was equipped with complete monitoring instruments to measure air pollutants, O_3 precursors, meteorological parameters, and photolysis rate. Strict quality control and quality assurance were applied to ensure the data validity in our study, and the detailed introductions of the monitoring procedure were also discussed in our previous studies (Hu et al., 2020; Wu et al., 2020).

2.2. Positive matrix factorization (PMF) model

A Positive Matrix Factorization model (PMF 5.0) has been repeatedly applied to identify the sources of HCHO (Chen et al., 2014; Ling et al., 2017; Yuan et al., 2013; Yuan et al., 2012; Zeng et al., 2019). The model

decomposes a speculated sample matrix into factor contributions and profiles, as shown in Eq. (1) (Liu et al., 2020):

$$e_{ij} = x_{ij} - \Sigma_{k=1}^{p} g_{ik} f_{kj} \quad (1)$$

where, e_{ij} represents the residual matrix for j species in i sample, x_{ij} is the measured concentration matrix of j species in i sample, g_{ik} is the factor contribution matrix of k source in i sample, and f_{kj} is the factor fraction matrix of j species in k source. The $Q(E)$, the model criteria, could evaluate the stability of the solution and be calculated as follows (Sarkar et al., 2017):

$$Q(E) = \Sigma_{i=1}^{n} \Sigma_{j=1}^{m} \left(\frac{e_{ij}}{s_{ij}} \right)^2 \quad (2)$$

where, s_{ij} is the standard deviation of j species in i sample, n and m represent the number of samples and species, respectively. The species inputted into the PMF model were mainly treated as important tracers of the pollution sources. The species uncertainties were needed to put into the model and calculated as Eq. (3), where, *EF* is the error factor, and MDL is the minimum detection limit. In our study, we chose HCHO, 17 VOCs, 1,2-dichloroethane, and O_3 to put into the PMF model, which are typical tracers of specific sources and have relatively high concentrations. Among them, O_3 is used as a surrogate to determine the fraction of HCHO secondary photochemical processes (Ling et al., 2017; Zeng et al., 2019).

$$u_{ij} = \sqrt{(EF \times conc.)^2 + (MDL)^2} \quad (3)$$

In this study, 4–6 factors were tested, and all runs converged. We selected the lowest Qrobust in each run of PMF for further examination. Table S5 shows the results of PMF of BS-DISP diagnostics. The $Q_{robust}/Q_{expected}$ increased from 4 factors to 6 factors. Displacement of factor elements (DISP) had no swaps for all factors, indicating that the solution was valid. The bootstrap (BS) of the results with 4 and 6 factors showed <80 % mapping for one factor. However, 5 factors had >90 % mapping, and ultimately 5 factors were the optimal solution. Anymore, the good correlations between the PMF model predicted and observed concentrations of each species were shown in Table S6. The correlation coefficients (R^2) were 0.76 for HCHO, 0.92 for O_3, 0.89 for 1,2-dichloroethane, and in the range of 0.60–0.99 for VOCs.

2.3. Chemical box model

A chemical box model, as one of the important methods for analyzing atmospheric chemical processes, was run based on the platform of the Framework for 0-Dimensional Atmospheric Modeling (F0AM), which has broad application potential in deeply exploring atmospheric observation data and comprehensively understanding the regional atmospheric pollution (Wolfe et al., 2016; Xia et al., 2022; Zhang et al., 2021c). About the chemical mechanism, the F0AM incorporating the latest chemical mechanism version of MCM-v3.3.1 (MCM, http://mcm.leeds.ac.uk/MCM/, last access: 13 May 2022) was applied to simulate the detailed photochemical processes and quantify the reaction rates of HCHO mechanism, and the MCM mechanism introduced 142 VOCs and about 20,000 chemical reactions (Jenkin et al., 2003). The physical process of dry deposition and atmospheric dilution within the boundary layer height was considered in the model (Li et al., 2018b; Liu et al., 2022a; Liu et al., 2022b). Therefore, the dry deposition velocity of some atmospheric reactants was shown in Table S7, which avoided the continuous accumulation of pollutant concentrations in the model (Sun et al., 2016; Zhang et al., 2003).

The observed trace gases (i.e., O_3, NO, NO_2, CO, SO_2, VOCs including HCHO, PAN, and HONO), photolysis rate constants ($JHCHO$, JO^1D, JNO_2, JH_2O_2, $JHONO$, and JNO_3), and meteorological parameters (i.e., RH, T, and P) with a time resolution of 1 h were put into the F0AM model, which was updated at 1 h intervals in the F0AM model to constrain and localize the model. Before running the model, the model was pre-run for 2 days to constrain the unmeasured species (e.g., OH, HO_2, and RO_2 radicals) reaching a steady state (Liu et al., 2022b).

The HCHO can affect O_3 formation and atmospheric oxidation capacity by radical chemistry (Li et al., 2014; Yang et al., 2020), hence the formation and loss of HCHO were discussed in our study. Furthermore, the HCHO sensitivities to their precursors were analyzed by relative incremental reactivity (RIR) (Eq. (4)) (Chen et al., 2020). P(HCHO) means the net production rate of HCHO, which was calculated by the differences between HCHO production rate and loss rate. The ΔX/X represents the reduction ratio of each targeted HCHO precursor group, and the value adopted is 20 %, which is of benefit for avoiding possible numerical calculation errors and minimizing interference with the model system (Yang et al., 2020).

$$\mathrm{RIR(HCHO)} = \frac{\Delta \mathrm{P(HCHO)}/\mathrm{P(HCHO)}}{\Delta \mathrm{X}/\mathrm{X}} \quad (4)$$

Comparing the modeled HCHO concentrations and observed HCHO concentrations would reflect the rationality of the model results, and the index of agreement (IOA) of 0.83 in spring and 0.80 in autumn in our study indicated that the model results were reasonably acceptable. The detailed model validation was shown in the supplement materials of Text 1, and the simulated and observed HCHO at the study site was shown in Fig. S1.

3. Results and discussion

3.1. Overview of observations

The occurrence of ambient HCHO, air pollutants, and meteorological parameters were shown in Fig. 1, and the related statistical information was summarized in Table S8. The average levels of the measured HCHO in spring and autumn were 2.9 ± 0.3 ppbv and 3.2 ± 1.4 ppbv, respectively. The HCHO level in Xiamen was lower than that in megacities, such as Guangzhou (summer: 9.3 ppbv) (Ling et al., 2017), Shenzhen (summer: 5.0 ppbv) (Wang et al., 2017), and Beijing (summer: 11.2 ppbv) (Yang et al., 2018), but was comparable to various coastal cities with relatively clean air, including Fuzhou (Spring: 2.5 ppbv) (He et al., 2020), Shantou (autumn: 4.1 ppbv) (Shen et al., 2021), and Hong Kong (spring: 3.4 ppbv) (Lui et al., 2017), indicating the influence of anthropogenic activities and photo-oxidation capacity. The concentrations of HCHO in this study were at a low level compared with these cities, which might be attributed to the relatively few sources of pollution emissions and beneficial diffusion conditions. Except for the concentrations of O_3 and HCHO, the concentrations of NO, NO_2, CO, PAN, and TVOCs in autumn were lower than those in spring (Table S8), suggesting the influence of the favorable accumulation conditions in spring and strong atmospheric oxidation capacity in autumn.

As shown in Fig. 1(b, d), the diurnal variations of HCHO presented an increasing trend after sunrise at 06:00 LT (local time), peaked in the afternoon (13:00 LT), and then gradually decreased after sunset. Although the measured HCHO exhibited similar single peak variations in both seasons, the HCHO mixing ratios kept a relatively high level during the nighttime (2.3 ppbv in spring and 2.5 ppbv in autumn) compared with those during the daytime (3.5 ppbv in spring and 4.0 ppbv in autumn), which were attributed to the replenishment of HCHO primary emissions and accumulation of pollutants. The conditional probability functions (CPF) polar plots (Fig. S2) revealed the relationship between high HCHO concentrations and wind (Uria-Tellaetxe and Carslaw, 2014; Zhang et al., 2021a), and the CPF results suggest that high HCHO values during the nighttime easily happened in the wind direction of the southeast with low wind speed (<2 $m{\cdot}s^{-1}$), showing the influence of urban plumes with intensive vehicle emissions from the downtown of Xiamen. Low wind speed at night (1.1 $m{\cdot}s^{-1}$ in spring and 1.7 $m{\cdot}s^{-1}$ in autumn) was favorable for the accumulation of air pollutants. The scatter plots of HCHO along with O_3 and PAN showed that O_3 and PAN had non-negligible relationships with HCHO in both seasons in Fig. S3, and similar diurnal patterns of HCHO, PAN, and O_3 verified the dominance of local photochemistry during the

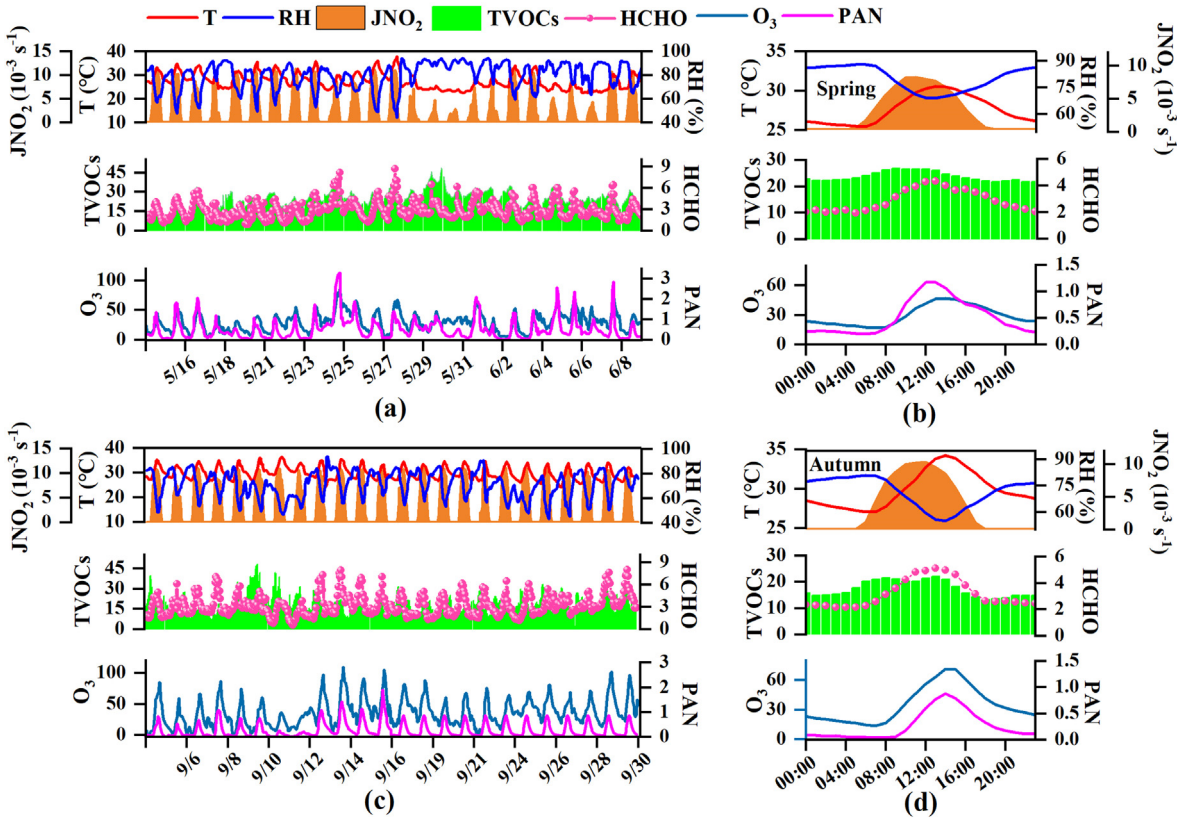

Fig. 1. Time series and average diurnal variations of measured HCHO, air pollutants (units: ppbv), meteorological parameters, and photolysis rate constants during (a, c) spring and (b, d) autumn.

observation period (de Blas et al., 2019; Wang et al., 2017), which was consistent with the findings in previous studies (Ling et al., 2017; Lui et al., 2017; Zhang et al., 2021c). In addition, the meteorological parameters (T, RH, and photolysis rate) in autumn had a significant difference from those in spring ($P < 0.05$, Table S9).

3.2. Source apportionment of HCHO

PMF was used to analyze the primary and secondary sources of HCHO. As shown in Fig. S4, five factors were identified by the PMF model. Factor 1 was characterized by a high load of O_3, attributed to intensive photochemical processes, that was, the secondary formation of HCHO (Li et al., 2010; Ling et al., 2017; Zeng et al., 2019). Meanwhile, secondary HCHO measured at the study site includes in-situ photochemical production and regional transport. Factor 2 had high loadings of 3-methylpentane, isopentane, the light hydrocarbons of n/iso-pentane and n/iso-butane, and aromatics. Therefore, factor 2 was defined as the source of vehicle exhaust (Li et al., 2017a; Liu et al., 2008). Factor 3 contributed significantly to alkenes and aromatics, such as propene, 1-butene, ethene, and benzene, which were the main VOC species in petrochemical industry (Guven and Olaguer, 2011; Sinha and Sinha, 2019). This factor was identified as industrial emission. Factor 4 was characterized by a high percentage of isoprene, and isoprene was an important precursor of HCHO (detailed discussion in Section 3.3.1). Thus, Factor 4 was designed as the biogenic source, which potentially produced HCHO from isoprene by photochemical reactions and was also belong to the secondary photochemical formation (Na et al., 2004; Sindelarova et al., 2022). Factor 5 had high loadings of toluene and 1,2-dichloroethane, which were widely used as industrial solvents and laboratory reagents (Mo et al., 2017). So, factor 5 was identified as solvent usage.

The percentages of different sources of ambient HCHO in spring and autumn were shown in Fig. 2. The contribution of secondary formation (49 % in spring and 46 % in autumn) to HCHO was the largest, comparable to other urban sites such as Guangzhou (53 %) (Ling et al., 2017) and Hong Kong (53 %) (Lui et al., 2017). Previous studies have reported that secondary photochemical formation was generally the main source of HCHO (34 % ~ 70 %) (Guven and Olaguer, 2011; Ling et al., 2017; Wang et al., 2017; Zeng et al., 2019). The contribution of HCHO from vehicle exhaust in spring (25 %) was higher than that in autumn (20 %), partly attributed to the unfavorable diffusion conditions in spring. According to backward trajectories analysis (Fig. S5), air mass (87 %) in spring originated from the southwest, which passed through Xiamen downtown areas with large amounts of vehicle exhaust emissions. The biogenic source contributed 18 % in spring and 24 % in autumn to the ambient HCHO, which consisted of isoprene levels. The industrial source in autumn was 1.5 times higher than that in spring, which could be attributed to long-range transport from the northeast. Backward trajectories (Fig. S5) in autumn showed 55 % air mass transport from the northeast, which brought pollutants from Quanzhou city, an industrial city adjacent to Xiamen. The contributions of solvent usage to HCHO seemed to be minor. Totally, secondary formation, vehicle exhaust, and biogenic source made significant contributions to HCHO with total contributions of 48 %, 23 %, and 21 %, respectively. In summary, the fractions of HCHO photochemical formation (including secondary formation and biogenic source) were 67 % in spring and 70 % in autumn. The results were similar to those at the urban sites (Zeng et al., 2019). In previous studies, secondary formation (53–75 %) and vehicle exhaust (14–31 %) was the dominant HCHO source in urban and suburban sites, while vehicle exhaust (47 %) in roadside sites was the dominant HCHO source, followed by secondary formation (43 %) (Guven and Olaguer, 2011; Ling et al., 2017; Zeng et al., 2019). Therefore, as one of the active OVOCs species, atmospheric HCHO depended on the emission of local sources, and the contributions of secondary formation have become particularly important under a certain season or intense photochemical reaction conditions (Chen et al., 2014; Zeng et al., 2019).

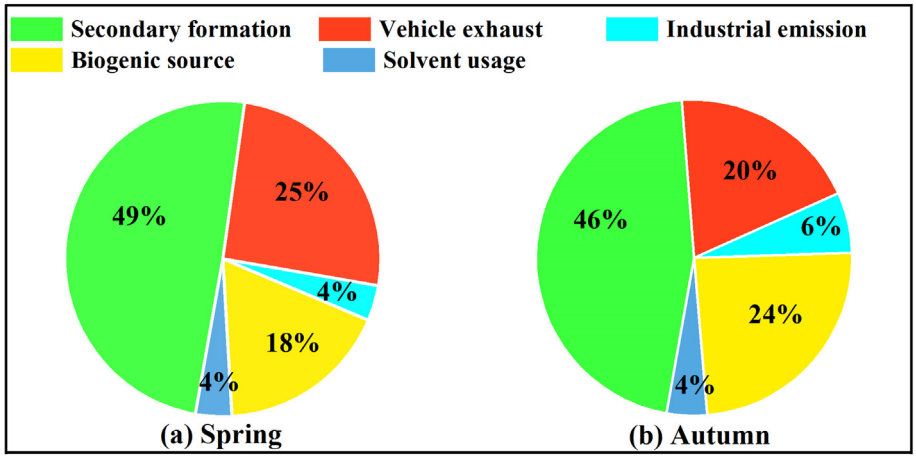

Fig. 2. Source contributions to HCHO levels in (a) spring and (a) autumn (note: the biogenic source was attributed to the secondary formation).

Yuan et al. (2012) proved the capacity of the PMF approach in identifying the role of chemical aging, and the abundance of VOCs in the PMF-aged factors could be reproduced by the photochemical aging of fresh factors. Considering the photochemical process impacts of the PMF factors, the relationship between the contribution of one factor to each species and its chemical reactivity (K_{OH}) was analyzed to separate factors that are associated with fresh and aged emissions (Chen et al., 2014; Yuan et al., 2012). The distribution of each species in the fresh factor would not correlate with its chemical reactivity, thus the HCHO distribution profile would be similar to that of each species in that factor. In the aged factors, the VOCs with more chemical activities would be more largely consumed by photochemical reactions, while the HCHO distribution profile would be higher than each species due to the secondary production. Fig. S6 showed relationships between the factor contributions to each species and K_{OH} values (representing chemical activities) for species. Indeed, the contributions of HCHO were higher than that of other species in factor 1 of secondary formation (the aged factor in Fig. S6a), but lower than or similar to other species in factors 2, 3, and 5 (the fresh factors in Fig. S6b, c, e). Factor 4 of biogenic source was thought as the aged factor because of the isoprene precursor for HCHO, thus the contributions of HCHO were relatively higher than other species (except isoprene) (Fig. S6d), furtherly confirming that PMF reasonably identified the contributions of primary and secondary sources of HCHO (Chen et al., 2014; Ling et al., 2017). In this study, we ran PMF models and discussed the apportionment results, indicating that the PMF approach can separate HCHO sources well.

3.3. HCHO formation mechanisms

3.3.1. HCHO in situ formation pathways

Fig. 3 shows the production and loss pathways of HCHO based on F0AM model. HCHO production rates during the daytime (06:00–17:00 LT) in spring and autumn were 1.9 ± 1.0 ppbv h^{-1} and 2.0 ± 1.8 ppbv h^{-1}, while HCHO loss rates were 1.8 ± 1.2 ppbv h^{-1} and 2.4 ± 1.8 ppbv h^{-1}, respectively. It should be noted that the 0-dimensional model only considers the photochemical reactions, dry deposition, and dilution mixing within the boundary layer, while the primary emissions of HCHO and the transport of air masses are not considered, and the model limitation leads to the discrepancy between the simulated and observed HCHO production (Fig. S1) (Yang et al., 2018; Yang et al., 2020; Zhang et al., 2021a). Although some bias exists, the model results still provide valuable information on secondary formation of HCHO in our study based on the model validation of IOA in our research.

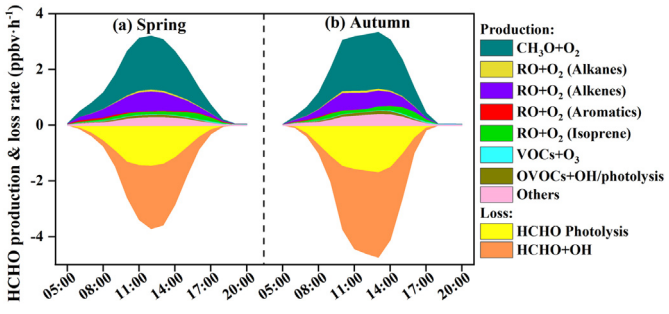

Fig. 3. Model-simulated in situ HCHO production rate and loss rate in (a) spring and (b) autumn.

The dominant pathway of daytime average HCHO production was the RO + O_2 reaction, which accounted for 87 % and 85 % of all HCHO production pathways in spring and autumn, respectively. After further refinement of the RO + O_2 reactions by classifying different RO first-generation precursors, the CH_3O + O_2 pathway contributed to total HCHO production rates mostly of 57 % in spring and 58 % in autumn. Moreover, RO derived from alkenes and isoprene reacting with O_2 contributed to total HCHO production of 21 % and 6 % in spring, and 18 % and 6 % in autumn, respectively, and the contributions of RO produced by alkanes and aromatics were <2 %. CH_3O radicals were from aromatics, alkenes, and isoprene, therefore, we provided a lower limit of the other pathways of RO + O_2 in this study (Yang et al., 2020; Zeng et al., 2019; Zhang et al., 2021b; Zhu et al., 2020). The 'others' category (detailed reactions shown in Table S10) accounted for 9 % and 11 % of the total production rate in spring and autumn, respectively. In previous studies, CH_3O + O_2 was also the dominant contributor to HCHO, followed by the RO from alkenes or isoprene (Zhang et al., 2021a; Zeng et al., 2019; Yang et al., 2020). Moreover, the isoprene degradation could be the dominant source of HCHO in rural and suburban areas with relatively high vegetation coverage, while the oxidation of alkenes in urban regions showed relatively high contributions to HCHO secondary formation, indicating the influence of urban plumes (Zhang et al., 2021a; Zeng et al., 2019; Yang et al., 2020; Yang et al., 2018; Li et al., 2014).

As for the loss pathways of HCHO, the reaction rates of HCHO + OH in spring and autumn were 1.0 ± 0.9 and 1.5 ± 1.2 ppbv h^{-1}, and the HCHO photolysis was 0.8 ± 0.5 and 1.0 ± 0.6 ppbv h^{-1}, respectively. It was worth noting that HCHO production rates had minor variations between spring and autumn, while the HCHO loss rates in autumn were significantly higher than those in spring ($P < 0.05$). Table S11 shows the comparisons of HCHO concentrations and formation rates in different cities, and he photolysis rates in Shanghai and Hong Kong were lower than those in Xiamen (Liu et al., 2022a), indicating that the favorable meteorological conditions not only made HCHO decomposition more competitive but also limited the high HCHO concentration. The results implied strong photochemical effects with high yields of ROx radical in autumn (the detailed description of ROx showed in Fig. 5).

3.3.2. Identification of key precursor species of HCHO

Sensitivity tests based on the F0AM model were furtherly carried out to quantify the potential influence of different precursors on HCHO formation (Luecken et al., 2018; Yang et al., 2020). Fig. 4 shows the relative incremental reactivity (RIR) for major groups and specific species of HCHO precursors. HCHO production was highly VOCs-sensitive with positive RIR values, indicating that reducing VOCs emissions might effectively inhibit the HCHO formation in Xiamen. As shown in Fig. 4a, the formation of HCHO was mainly controlled by alkenes with the largest RIR values in spring (1.2) and autumn (1.1), followed by isoprene (0.6 in spring and 0.8 in autumn), aromatics (0.8, 0.6), and alkanes (0.5, 0.4). The results suggested that both biogenic and anthropogenic emissions might influence the HCHO secondary formation. In addition, the RIR of isoprene in spring was lower than that in autumn, which was attributed to isoprene concentrations affected by solar radiation and air temperature (de Blas et al., 2019).

Based on the explicit mechanism in the model, HCHO precursors at the species level could be further identified. In this study, the impact of anthropogenic precursors on HCHO was mainly discussed. Alkenes and aromatics made the greatest contributions to HCHO formation among the top 10 VOCs species (Fig. 4b). The top 5 species of RIR were propene (0.4 in spring and 0.3 in autumn), ethene (0.4, 0.2), toluene (0.3, 0.2), m/p-xylene (0.2, 0.1), and trans-2-butene (0.2, 0.2), which were mainly from vehicle exhaust, biomass burning, and solvent usage (Ling et al., 2017). These results showed that reducing anthropogenic emissions of the top 5 species could decline both HCHO and O_3 production.

3.4. Contribution of HCHO to atmospheric photochemistry

3.4.1. Impacts on atmospheric oxidation capacity

The atmospheric oxidation capacity (AOC) is a crucial aspect of exploring the complex atmospheric photochemistry processes, reflecting the essential driving force in the loss of primary components and the production of secondary pollutants in tropospheric chemistry (Chen et al., 2020). AOC was defined as the sum of oxidation rates in converting primary pollutants (CO, VOCs, etc.) into secondary pollutants by the major oxidants (i.e., OH, NO_3, O_3) (Xue et al., 2016). Fig. S7 shows the diurnal patterns of the model-calculated AOC during the observation period. The daily maximum AOC was shown at around 12:00 LT with levels of 1.2×10^8 molecules cm^{-3} s^{-1} in spring and 1.5×10^8 molecules cm^{-3} s^{-1}in autumn, which was comparable to that in the suburban site of the YRD region (1.2×10^8 molecules cm^{-3} s^{-1}), higher than that in a regional background in Hong Kong (6.2×10^7 molecules cm^{-3} s^{-1}) and a rural site with much low pollution sources in Berlin (1.4×10^7 molecules cm^{-3} s^{-1}), but lower than that in some cities, such as Santiago (3.2×10^8 molecules cm^{-3} s^{-1}) (Geyer et al., 2001; Xue et al., 2016; Zhang et al., 2021a; Zhu et al., 2020).

The AOC levels in different regions were mainly controlled by the precursors and photochemical conditions, such as solar radiation and air temperature. As Fig. S7 shows, the OH played a dominant role in contribution to AOC during the daytime, accounting for around 97 % of total AOC, then O_3 and NO_3 contributed 2 % and 3 % in both seasons. During the nighttime, NO_3 (71 % in spring and 66 % in autumn) contributed the most, followed by OH (15 % and 21 %) and O_3 (14% and 13 %). In particular, the AOC by NO_3 contributed to the maximum at around 19:00 LT of 84 % in spring and 71 % in autumn, when relatively high concentrations of O_3 and NO_2 with weak solar radiation accelerated the formation and accumulation of NO_3 (Fig. 1) (Chen et al., 2020; Geyer et al., 2001). The AOC levels in autumn were 1.2– 1.4 times higher than that in spring, due to the favorable photochemical conditions. And, the main contributor of AOC was OH radicals, which greatly caused the production of secondary pollutants.

OH reactivity was used to compare the importance of different reactants to the OH loss, which has been widely used as an indicator of the intensity of atmospheric oxidation capacity (Mao et al., 2010; Xue et al., 2016). The OH reactivity includes the OH oxidation of both measured VOCs (such as C_2-C_{10} hydrocarbons, and measured carbonyls) and modeled compounds (mainly including unmeasured higher OVOCs), and the OH reactivity from the measured compounds accounted for the majority of the total OH reactivity of VOCs. The average values of OH reactivity were 5.4 s^{-1} in spring and 4.1 s^{-1} in autumn (Fig. 5), which were much lower than those in polluted urban regions, but higher than that in remote or background sites (Kovacs et al., 2003; Lou et al., 2010; Ren et al., 2005; Zhu et al., 2020). The simulated OH reactivity in our study was within the measured range of other sites in China (Fuchs et al., 2017; Yang et al., 2016). Oxygenated volatile organic compounds (OVOCs, 72 % in spring and 75 % in autumn) covered large fractions of OH reactivity, followed by alkenes (13 %, 11 %), alkanes (8 %, 8 %), and aromatics (7 %, 5 %). It should be noted that HCHO accounted for 28 % in spring and 34 % in autumn of the OH reactivity by OVOCs, and contributed 20 % in spring and 25 % in autumn to the total OH reactivity, elucidating the significance of HCHO in photochemistry. A previous study also showed the importance of HCHO in atmospheric radicals of HO_2 and O_3 formation (Zeng et al., 2019).

3.4.2. Impacts on the radical chemistry

HCHO modulates O_3 formation mainly by controlling the radical recycling in the troposphere (Huang et al., 2009; Zeng et al., 2019; Zhang et al., 2022). To furtherly quantify the varieties in ROx chemistry and O_3 formation in response to HCHO chemistry, two parallel scenarios were conducted through the F0AM model. One scenario was run with all MCM mechanism defined as AS, and the other was run with the HCHO mechanism disabled in MCM mechanism defined as DS. Considering the numerous chemical formation reactions of HCHO, our study mainly disabled the

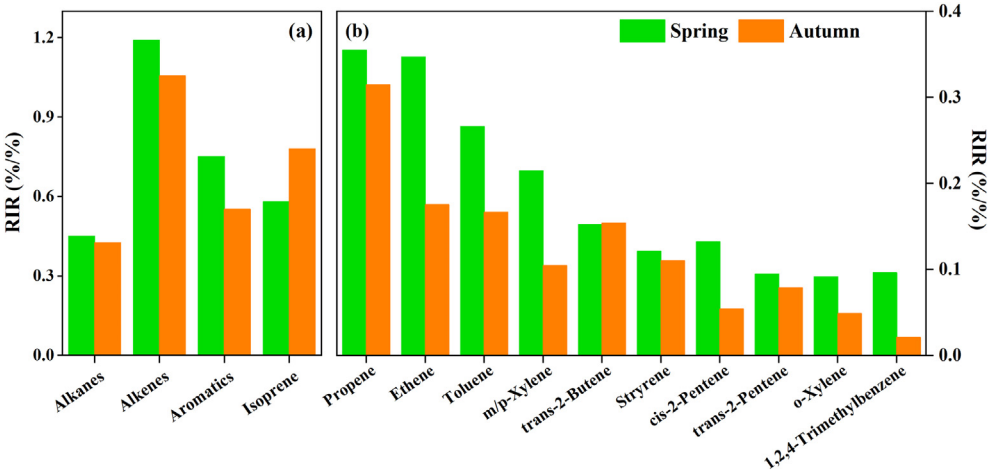

Fig. 4. The model calculated relative incremental reactivity (RIR) for (a) major HCHO precursor groups and (b) the top 10 specific species in spring and autumn during the daytime (06:00–17:00 LT).

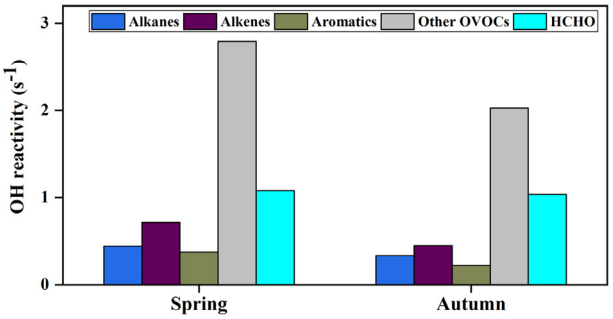

Fig. 5. The model-calculated values of OH reactivity in spring and autumn.

HCHO loss pathways of HCHO photolysis, HCHO + OH, and HCHO + NO_3, which makes HCHO become a stable secondary pollutant that will not continue to react, thus the HCHO loss pathways were disabled in DS scenario.

The differences in ROx levels and production pathways in model scenarios of AS and DS were analyzed to investigate the chain effect of HCHO on ROx cycling (Figs. 6, 7, and Table S12). The daytime average OH decreased by 25 % in spring and 16 % in autumn when HCHO mechanism was disabled, and the OH production pathway of HO_2 + NO was mainly slowed down by 35 % in spring and 30 % in autumn. The changes of O_3 photolysis (spring: 0.06 ppbv h^{-1}, autumn: 0.08 ppbv h^{-1}) and HONO photolysis (0.06 ppbv h^{-1}, autumn: 0.04 ppbv h^{-1}) from AS to DS were minor, and the contribution of the slow reaction rates of O_3 + VOCs, HNO_3 photolysis, H_2O_2 photolysis, and OVOCs photolysis (<0.02 ppbv h^{-1}) could be ignored in both AS and DS scenarios. The daytime average HO_2 decreased by 45 % in spring and 40 % in autumn from AS to DS. Except for the O_3 + VOCs, the other HO_2 production pathways of OH + CO, RO_2 + NO, OH + VOCs, HCHO photolysis, and OVOCs photolysis showed relatively high contributions. Among them, the difference in HCHO photolysis between AS and DS was most with 100 % reduction of HO_2 production, followed by OH + VOCs (84 % in both seasons), OH + CO (26 % in spring and 17 % in autumn), RO_2 + NO (11 %, 6 %). In Zeng et al. (2019) study, HCHO photochemical reactions (including HCHO photolysis and OH + HCHO) had a non-negligible contribution to HO_2 production in an urban site, accounting for 11 % of total HO_2 production rates and was significantly lower than that in our study (26 %). The daytime average RO_2 decreased by 26 % in spring and 19 % in autumn from AS to DS. Similar to the analysis above, OH + VOCs and OVOCs photolysis represented remarkable importance in RO_2 production. The deletion of the HCHO loss reactions also led to some reductions in the daytime reaction rate of OH + VOCs (19 % in spring and 10 % in autumn), and the changes of OVOCs photolysis NO_3 + VOCs and O_3 + VOCs were slight.

In general, disabling the HCHO mechanism would decrease the OH and RO_2 concentrations due to the weakened radical propagation efficiencies of HO_2 + NO → OH and OH + VOCs → RO_2, and would decrease the HO_2 concentrations by both HCHO photolysis and radical propagation. Thus, the differences in HO_2 between AS and DS were the highest, followed by RO_2 and OH. In our study, disabling HCHO mechanism decreased the ROx concentrations by 38 % in spring and 33 % in autumn and further reduced the O_3 formation, reflecting the significance of HCHO in photochemistry in the coastal site.

3.4.3. Impacts on the formation of O_3

To investigate the impacts of HCHO on O_3 formation during the observation period, the detailed O_3 production and loss pathways in both AS and DS were quantified (Fig. 8 and Table S13). The daytime production rates of HO_2 + NO and RO_2 + NO in AS were 7.8 and 3.0 ppbv h^{-1} in spring and 8.6 and 2.8 ppbv h^{-1} in autumn. Meanwhile, OH + NO_2 was the predominant O_3 loss reaction accounting for 60 % in spring and 60 % in autumn, followed by O_3 photolysis (22 % in spring and 29 % in autumn), RO_2 + NO_2 (8 %, 7 %), O_3 + HO_2 (3 %, 8 %), and O_3 + OH (3 %, 6 %), while the contributions of O_3 + VOCs and NO_3 + VOCs pathways were very limited. According to the differences between AS and DS, disabling HCHO mechanism could reduce the production rates of HO_2 + NO by 35 % in spring and 30 % in autumn, and decrease RO_2 + NO by 13 % and 6 %. About the O_3 loss pathways, the differences mainly reduced the rates of OH + NO_2 by 21 % in spring and 13 % in autumn, weakened RO_2 + NO_2 by 62 % and 19 %, lessened O_3 + HO_2 by 50 % and 43 %, and dropped O_3 + OH by 31 % and 19 %. The peak net O_3 rates decreased by 32 % in spring and 23 % in autumn. In Zeng et al. (2019) study, the difference in peak net O_3 rate was 17 % in a typical urban site through diminishing HCHO and was significantly lower than our results.

The contributions of HO_2 + NO, RO_2 + NO_2, O_3 + HO_2, O_3 + OH, and OH + NO_2 showed significant changes from AS to DS, and these reactions were mainly dominated by radical propagation pathways. Ultimately, the daytime average values of net O_3 production rates decreased by 32 % in spring and 29 % in autumn through disabling HCHO mechanism, and

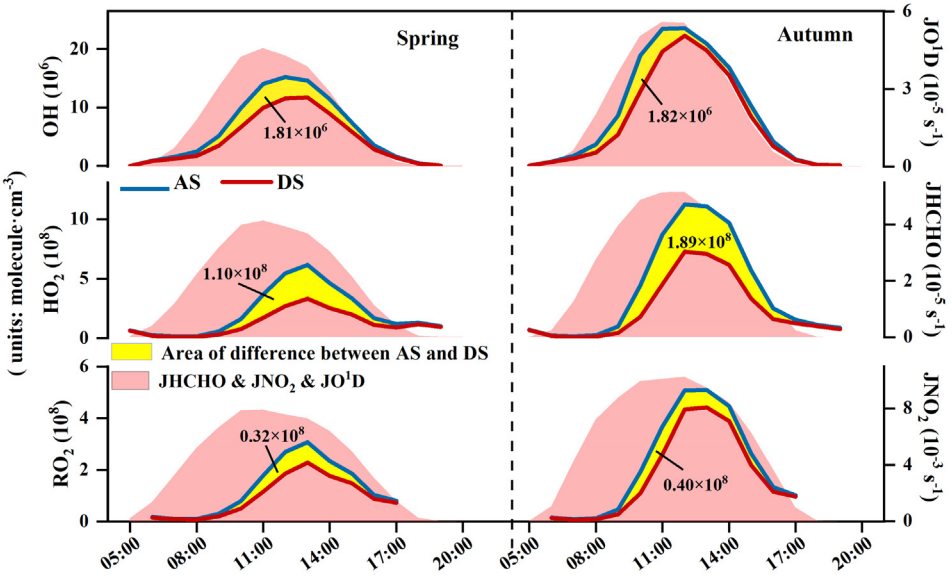

Fig. 6. The diurnal patterns and differences of OH, HO_2, and RO_2 radicals in model scenarios of AS and DS in (a) spring and (b) autumn. AS scenario was run with all MCM mechanism, and DS scenario was run with the HCHO mechanism disabled in MCM mechanism.

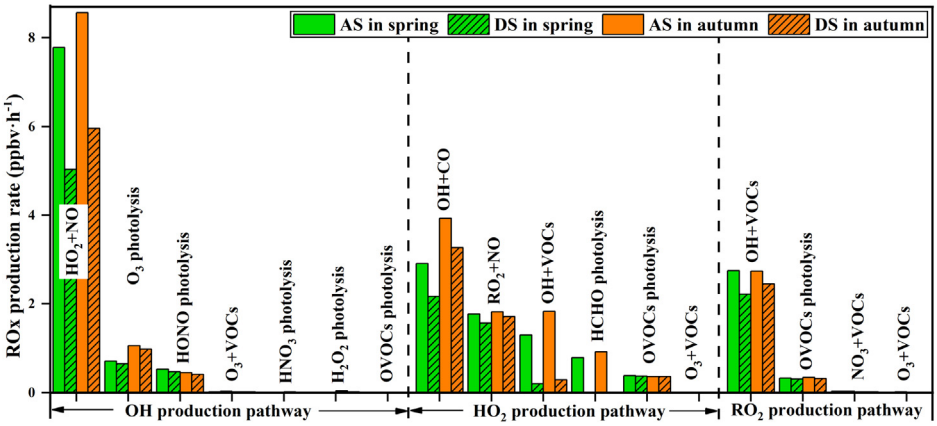

Fig. 7. The average daytime (06:00–17:00) production rates of OH, HO_2, and RO_2 in model scenarios of AS and DS. AS scenario was run with all MCM mechanism, and DS scenario was run with the HCHO mechanism disabled in MCM mechanism.

these were attributed to the drop in ROx concentrations or radical propagation rates. The results highlighted and quantified the important impacts of HCHO on O_3 formation in the southeast coastal area.

4. Conclusions

Field observations and model analyses were carried out in a coastal city with frequent photochemical pollution. We found that secondary formation of O_3 and HCHO in autumn was stronger than those in spring, relating to the intensive photochemical reaction and meteorological conditions. However, the elevated loss rates of HCHO in autumn indicated that strong photochemical conditions not only enhance the production of HCHO but also constrain high HCHO levels. Secondary photochemical formation made the largest contributions to ambient HCHO in the coastal city. The sensitivity analysis suggested that alkenes and aromatics were the most important precursors to HCHO, the top 5 precursors at the species level contributing to HCHO were propene, ethene, toluene, m/p-xylene, and trans-2-butene, which were mainly emitted from combustion sources and solvent use.

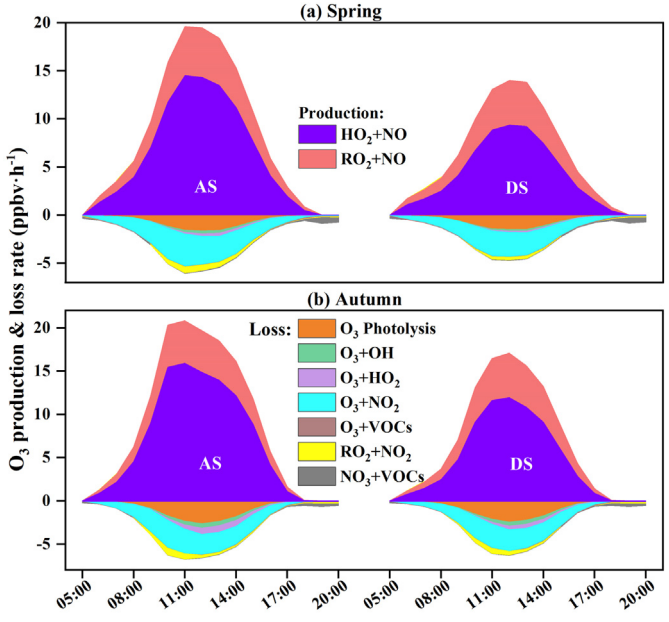

Fig. 8. Simulated profiles of O_3 mechanism in AS and DS in (a) spring and (b) autumn. AS scenario was run with all MCM mechanism, and DS scenario was run with the HCHO mechanism disabled in MCM mechanism.

Based on the model analysis, we verified that HCHO mechanism increased the ROx concentrations by 36 %, and increased net O_3 production rates by 31 %, reflecting the significance of HCHO in photochemistry. For the O_3 formation mechanism, HCHO mechanism improved the production rates of HO_2 + NO and RO_2 + NO, and the O_3 loss pathways of OH + NO_2, RO_2 + NO_2, O_3 + HO_2, and O_3 + OH, indicating that the HCHO affected O_3 formation mechanism by controlling the efficiencies of radical propagation. In a word, the pollution characteristics and photochemical effects of HCHO provided significant guidance for future photochemical pollution control in relatively clean areas, and the impacts of meteorological conditions brought by synoptic patterns (such as subtropical high) on the photochemical pollution could not be ignored.

CRediT authorship contribution statement

Taotao Liu collected the data, contributed to the data analysis and performed chemical modeling analyses, and wrote the paper. Jinsheng Chen designed the manuscript and supported funding of observation and research. Yiling Lin collected the data. Youwei Hong revised the manuscript. Gaojie Chen, Chen Yang, Lingling Xu, Mengren Li, Xiaolong Fan contributed to discussions of results. Fuwang Zhang provided part of the data in Xiamen.

Data availability

Data will be made available on request.

Declaration of competing interest

The authors declare that they have no known competing financial interests or personal relationships that could have appeared to influence the work reported in this paper.

Acknowledgment

This study was funded by the National Natural Science Foundation of China (U22A20578), the Science and Technology Department of Fujian Province (2022L3025), the Cultivating Project of Strategic Priority Research Program of Chinese Academy of Sciences (XDPB1903), the Foreign Cooperation Project of Fujian Province (2020I0038), the Xiamen Youth Innovation Fund Project (3502Z20206094), the FJIRSM&IUE Joint Research Fund (RHZX-2019-006), Center for Excellence in Regional Atmospheric Environment project (E0L1B20201), Xiamen Atmospheric Environment Observation and Research Station of Fujian Province, and Fujian Key Laboratory of Atmospheric Ozone Pollution Prevention (Institute of Urban Environment, Chinese Academy of Sciences).

Appendix A. Supplementary data

Supplementary data to this article can be found online at https://doi.org/10.1016/j.scitotenv.2022.160210.

References

Anderson, D.C., Nicely, J.M., Wolfe, G.M., Hanisco, T.F., Salawitch, R.J., Canty, T.P., Dickerson, R.R., Apel, E.C., Baidar, S., Bannan, T.J., Blake, N.J., Chen, D., Dix, B., Fernandez, R.P., Hall, S.R., Hornbrook, R.S., Huey, L.G., Josse, B., Joeckel, P., Kinnison, D.E., Koenig, T.K., Le Breton, M., Marecal, V., Morgenstern, O., Oman, L.D., Pan, L.L., Percival, C., Plummer, D., Revell, L.E., Rozanov, E., Saiz-Lopez, A., Stenke, A., Sudo, K., Tilmes, S., Ullmann, K., Volkamer, R., Weinheimer, A.J., Zeng, G., 2017. Formaldehyde in the tropical Western Pacific: chemical sources and sinks, convective transport, and representation in CAM-Chem and the CCMI models. J. Geophys. Res. Atmos. 122, 11201–11226.

Bao, J., Li, H., Wu, Z., Zhang, X., Zhang, H., Li, Y., Qian, J., Chen, J., Deng, L., 2022. Atmospheric carbonyls in a heavy ozone pollution episode at a metropolis in Southwest China: characteristics, health risk assessment, sources analysis. J. Environ. Sci. (China) 113, 40–54.

Chen, T., Xue, L., Zheng, P., Zhang, Y., Liu, Y., Sun, J., Han, G., Li, H., Zhang, X., Li, Y., Li, H., Dong, C., Xu, F., Zhang, Q., Wang, W., 2020. Volatile organic compounds and ozone air pollution in an oil production region in northern China. Atmos. Chem. Phys. 20, 7069–7086.

Chen, W.T., Shao, M., Lu, S.H., Wang, M., Zeng, L.M., Yuan, B., Liu, Y., 2014. Understanding primary and secondary sources of ambient carbonyl compounds in Beijing using the PMF model. Atmos. Chem. Phys. 14, 3047–3062.

Cheng, Y., Lee, S.C., Huang, Y., Ho, K.F., Ho, S.S.H., Yau, P.S., Louie, P.K.K., Zhang, R.J., 2014. Diurnal and seasonal trends of carbonyl compounds in roadside, urban, and suburban environment of Hong Kong. Atmos. Environ. 89, 43–51.

de Blas, M., Ibanez, P., Garcia, J.A., Gomez, M.C., Navazo, M., Alonso, L., Durana, N., Iza, J., Gangoiti, G., de Camara, E.S., 2019. Summertime high resolution variability of atmospheric formaldehyde and non-methane volatile organic compounds in a rural background area. Sci. Total Environ. 647, 862–877.

Edwards, P.M., Brown, S.S., Roberts, J.M., Ahmadov, R., Banta, R.M., deGouw, J.A., Dube, W.P., Field, R.A., Flynn, J.H., Gilman, J.B., Graus, M., Helmig, D., Koss, A., Langford, A.O., Lefer, B.L., Lerner, B.M., Li, R., Li, S.M., McKeen, S.A., Murphy, S.M., Parrish, D.D., Senff, C.J., Soltis, J., Stutz, J., Sweeney, C., Thompson, C.R., Trainer, M.K., Tsai, C., Veres, P.R., Washenfelder, R.A., Warneke, C., Wild, R.J., Young, C.J., Yuan, B., Zamora, R., 2014. High winter ozone pollution from carbonyl photolysis in an oil and gas basin. Nature 514, 351–354.

Fuchs, H., Tan, Z., Lu, K., Bohn, B., Broch, S., Brown, S.S., Dong, H., Gomm, S., Häseler, R., He, L., Hofzumahaus, A., Holland, F., Li, X., Liu, Y., Lu, S., Min, K.-E., Rohrer, F., Shao, M., Wang, B., Wang, M., Wu, Y., Zeng, L., Zhang, Y., Wahner, A., Zhang, Y., 2017. OH reactivity at a rural site (Wangdu) in the North China Plain: contributions from OH reactants and experimental OH budget. Atmos. Chem. Phys. 17, 645–661.

Geyer, A., Alicke, B., Konrad, S., Schmitz, T., Stutz, J., Platt, U., 2001. Chemistry and oxidation capacity of the nitrate radical in the continental boundary layer near Berlin. J. Geophys. Res.-Atmos. 106, 8013–8025.

Glowania, M., Rohrer, F., Dorn, H.-P., Hofzumahaus, A., Holland, F., Kiendler-Scharr, A., Wahner, A., Fuchs, H., 2021. Comparison of formaldehyde measurements by Hantzsch, CRDS and DOAS in the SAPHIR chamber. Atmos. Meas. Tech. 14, 4239–4253.

Guo, H., Jiang, F., Cheng, H.R., Simpson, I.J., Wang, X.M., Ding, A.J., Wang, T.J., Saunders, S.M., Wang, T., Lam, S.H.M., Blake, D.R., Zhang, Y.L., Xie, M., 2009. Concurrent observations of air pollutants at two sites in the Pearl River Delta and the implication of regional transport. Atmos. Chem. Phys. 9, 7343–7360.

Guven, B.B., Olaguer, E.P., 2011. Ambient formaldehyde source attribution in Houston during TexAQS II and TRAMP. Atmos. Environ. 45, 4272–4280.

He, Z., Zhang, X., Li, Y., Zhong, X., Li, H., Gao, R., Li, J., 2020. Characterizing carbonyl compounds and their sources in Fuzhou ambient air, southeast of China. PeerJ 8, e10227.

Hu, B., Liu, T., Hong, Y., Xu, L., Li, M., Wu, X., Wang, H., Chen, J., Chen, J., 2020. Characteristics of peroxyacetyl nitrate (PAN) in a coastal city of southeastern China: photochemical mechanism and pollution process. Sci. Total Environ. 719, 137493.

Hu, D., Tobon, Y., Agostini, A., Grosselin, B., Chen, Y., Robin, C., Yahyaoui, A., Colin, P., Mellouki, A., Daele, V., 2022. Diurnal variation and potential sources of indoor formaldehyde at elementary school, high school and university in the Centre Val de Loire region of France. Sci. Total Environ. 811, 152271.

Huang, J., Feng, Y., Li, J., Xiong, B., Feng, J., Wen, S., Sheng, G., Fu, J., Wu, M., 2009. Characteristics of carbonyl compounds in ambient air of Shanghai, China. J. Atmos. Chem. 61, 1–20.

Jenkin, M.E., Saunders, S.M., Wagner, V., Pilling, M.J., 2003. Protocol for the development of the Master Chemical Mechanism, MCM v3 (Part B): tropospheric degradation of aromatic volatile organic compounds. Atmos. Chem. Phys. 3, 181–193.

Kovacs, T.A., Brune, W.H., Harder, H., Martinez, M., Simpas, J.B., Frost, G.J., Williams, E., Jobson, T., Stroud, C., Young, V., Fried, A., Wert, B., 2003. Direct measurements of urban OH reactivity during Nashville SOS in summer 1999. J. Environ. Monit. 5, 68–74.

Li, B., Ho, S.S.H., Xue, Y., Huang, Y., Wang, L., Cheng, Y., Dai, W., Zhong, H., Cao, J., Lee, S., 2017a. Characterizations of volatile organic compounds (VOCs) from vehicular emissions at roadside environment: the first comprehensive study in Northwestern China. Atmos. Environ. 161, 1–12.

Li, P., Wang, L., Guo, P., Yu, S., Mehmood, K., Wang, S., Liu, W., Seinfeld, J.H., Zhang, Y., Wong, D.C., Alapaty, K., Pleim, J., Mathur, R., 2017b. High reduction of ozone and particulate matter during the 2016 G-20 summit in Hangzhou by forced emission controls of industry and traffic. Environ. Chem. Lett. 15, 709–715.

Li, Q., Zhang, L., Wang, T., Wang, Z., Fu, X., Zhang, Q., 2018a. "New" reactive nitrogen chemistry reshapes the relationship of ozone to its precursors. Environ. Sci. Technol. 52, 2810–2818.

Li, X., Rohrer, F., Brauers, T., Hofzumahaus, A., Lu, K., Shao, M., Zhang, Y.H., Wahner, A., 2014. Modeling of HCHO and CHOCHO at a semi-rural site in southern China during the PRIDE-PRD2006 campaign. Atmos. Chem. Phys. 14, 12291–12305.

Li, Y., Shao, M., Lu, S., Chang, C.-C., Dasgupta, P.K., 2010. Variations and sources of ambient formaldehyde for the 2008 Beijing Olympic games. Atmos. Environ. 44, 2632–2639.

Li, Z., Xue, L., Yang, X., Zha, Q., Tham, Y.J., Yan, C., Louie, P.K.K., Luk, C.W.Y., Wang, T., Wang, W., 2018b. Oxidizing capacity of the rural atmosphere in Hong Kong, Southern China. Sci. Total Environ. 612, 1114–1122.

Ling, Z.H., Zhao, J., Fan, S.J., Wang, X.M., 2017. Sources of formaldehyde and their contributions to photochemical O3 formation at an urban site in the Pearl River Delta, southern China. Chemosphere 168, 1293–1301.

Liu, T., Chen, G., Chen, J., Xu, L., Li, M., Hong, Y., Chen, Y., Ji, X., Yang, C., Chen, Y., Huang, W., Huang, Q., Wang, H., 2022a. Seasonal characteristics of atmospheric peroxyacetyl nitrate (PAN) in a coastal city of Southeast China: explanatory factors and photochemical effects. Atmos. Chem. Phys. 22, 4339–4353.

Liu, T., Hong, Y., Li, M., Xu, L., Chen, J., Bian, Y., Yang, C., Dan, Y., Zhang, Y., Xue, L., Zhao, M., Huang, Z., Wang, H., 2022b. Atmospheric oxidation capacity and ozone pollution mechanism in a coastal city of southeastern China: analysis of a typical photochemical episode by an observation-based model. Atmos. Chem. Phys. 22, 2173–2190.

Liu, T., Hu, B., Yang, Y., Li, M., Hong, Y., Xu, X., Xu, L., Chen, N., Chen, Y., Xiao, H., Chen, J., 2020. Characteristics and source apportionment of PM2.5 on an island in Southeast China: impact of sea-salt and monsoon. Atmos. Res. 235, 104786.

Liu, Y., Shao, M., Fu, L., Lu, S., Zeng, L., Tang, D., 2008. Source profiles of volatile organic compounds (VOCs) measured in China: part I. Atmos. Environ. 42, 6247–6260.

Liu, Y., Yuan, B., Li, X., Shao, M., Lu, S., Li, Y., Chang, C.C., Wang, Z., Hu, W., Huang, X., He, L., Zeng, L., Hu, M., Zhu, T., 2015. Impact of pollution controls in Beijing on atmospheric oxygenated volatile organic compounds (OVOCs) during the 2008 Olympic Games: observation and modeling implications. Atmos. Chem. Phys. 15, 3045–3062.

Lou, S., Holland, F., Rohrer, F., Lu, K., Bohn, B., Brauers, T., Chang, C.C., Fuchs, H., Haeseler, R., Kita, K., Kondo, Y., Li, X., Shao, M., Zeng, L., Wahner, A., Zhang, Y., Wang, W., Hofzumahaus, A., 2010. Atmospheric OH reactivities in the Pearl River Delta - China in summer 2006: measurement and model results. Atmos. Chem. Phys. 10, 11243–11260.

Louie, P.K.K., Ho, J.W.K., Tsang, R.C.W., Blake, D.R., Lau, A.K.H., Yu, J.Z., Yuan, Z., Wang, X., Shao, M., Zhong, L., 2013. VOCs and OVOCs distribution and control policy implications in Pearl River Delta region,China. Atmos. Environ. 76, 125–135.

Lowe, D.C., Schmidt, U., 1983. Formaldehyde (HCHO) measurements in the nonurban atmosphere. J. Atmos. Chem. 88, 10844.

Luecken, D.J., Napelenok, S.L., Strum, M., Scheffe, R., Phillips, S., 2018. Sensitivity of ambient atmospheric formaldehyde and ozone to precursor species and source types across the United States. Environ. Sci. Technol. 52, 4668–4675.

Lui, K.H., Ho, S.S.H., Louie, P.K.K., Chan, C.S., Lee, S.C., Hu, D., Chan, P.W., Lee, J.C.W., Ho, K.F., 2017. Seasonal behavior of carbonyls and source characterization of formaldehyde (HCHO) in ambient air. Atmos. Environ. 152, 51–60.

Mao, J., Ren, X., Chen, S., Brune, W.H., Chen, Z., Martinez, M., Harder, H., Lefer, B., Rappenglück, B., Flynn, J., Leuchner, M., 2010. Atmospheric oxidation capacity in the summer of Houston 2006: comparison with summer measurements in other metropolitan studies. Atmos. Environ. 44, 4107–4115.

Mo, Z., Shao, M., Lu, S., Niu, H., Zhou, M., Sun, J., 2017. Characterization of non-methane hydrocarbons and their sources in an industrialized coastal city, Yangtze River Delta, China. Sci. Total. Environ. 593–594, 641–653.

Na, K., Kim, Y.P., Moon, I., Moon, K.-C., 2004. Chemical composition of major VOC emission sources in the Seoul atmosphere. Chemosphere 55, 585–594.

Nussbaumer, C.M., Crowley, J.N., Schuladen, J., Williams, J., Hafermann, S., Reiffs, A., Axinte, R., Harder, H., Ernest, C., Novelli, A., Sala, K., Martinez, M., Mallik, C., Tomsche, L., Plass-Dülmer, C., Bohn, B., Lelieveld, J., Fischer, H., 2021. Measurement report: photochemical production and loss rates of formaldehyde and ozone across Europe. Atmos. Chem. Phys. 21, 18413–18432.

Ou, J., Yuan, Z., Zheng, J., Huang, Z., Shao, M., Li, Z., Huang, X., Guo, H., Louie, P.K., 2016. Ambient ozone control in a photochemically active region: short-term despiking or long-term attainment? Environ. Sci. Technol. 50, 5720–5728.

Ren, X.R., Brune, W.H., Cantrell, C.A., Edwards, G.D., Shirley, T., Metcalf, A.R., Lesher, R.L., 2005. Hydroxyl and peroxy radical chemistry in a rural area of Central Pennsylvania: observations and model comparisons. J. Atmos. Chem. 52, 231–257.

Sarkar, C., Sinha, V., Sinha, B., Panday, A.K., Rupakheti, M., Lawrence, M.G., 2017. Source apportionment of NMVOCs in the Kathmandu Valley during the SusKat-ABC international field campaign using positive matrix factorization. Atmos. Chem. Phys. 17, 8129–8156.

Shen, H., Liu, Y., Zhao, M., Li, J., Zhang, Y., Yang, J., Jiang, Y., Chen, T., Chen, M., Huang, X., Li, C., Guo, D., Sun, X., Xue, L., Wang, W., 2021. Significance of carbonyl compounds to photochemical ozone formation in a coastal city (Shantou) in eastern China. Sci. Total Environ. 764, 144031.

Sindelarova, K., Markova, J., Simpson, D., Huszar, P., Karlicky, J., Darras, S., Granier, C., 2022. High-resolution biogenic global emission inventory for the time period 2000–2019 for air quality modelling. Earth Syst. Sci. Data 14, 251–270.

Sinha, B., Sinha, V., 2019. Source apportionment of volatile organic compounds in the northwest Indo-Gangetic Plain using a positive matrix factorization model. Atmos. Chem. Phys. 19, 15467–15482.

Sun, L., Xue, L., Wang, T., Gao, J., Ding, A., Cooper, O.R., Lin, M., Xu, P., Wang, Z., Wang, X., Wen, L., Zhu, Y., Chen, T., Yang, L., Wang, Y., Chen, J., Wang, W., 2016. Significant increase of summertime ozone at Mount Tai in Central Eastern China. Atmos. Chem. Phys. 16, 10637–10650.

Uria-Tellaetxe, I., Carslaw, D.C., 2014. Conditional bivariate probability function for source identification. Environ. Model. Softw. 59, 1–9.

Villanueva, F., Lara, S., Amo-Salas, M., Cabañas, B., Martín, P., Salgado, S., 2021. Investigation of formaldehyde and other carbonyls in a small urban atmosphere using passive samplers.A comprehensive data analysis. Microchem. J. 167, 106270.

Wang, C., Huang, X.-F., Han, Y., Zhu, B., He, L.-Y., 2017. Sources and potential photochemical roles of formaldehyde in an urban atmosphere in South China. J. Geophys. Res. Atmos. 122, 11,934–911,947.

Wang, H., Lyu, X., Guo, H., Wang, Y., Zou, S., Ling, Z., Wang, X., Jiang, F., Zeren, Y., Pan, W., Huang, X., Shen, J., 2018. Ozone pollution around a coastal region of South China Sea: interaction between marine and continental air. Atmos. Chem. Phys. 18, 4277–4295.

Wolfe, G.M., Kaiser, J., Hanisco, T.F., Keutsch, F.N., de Gouw, J.A., Gilman, J.B., Graus, M., Hatch, C.D., Holloway, J., Horowitz, L.W., Lee, B.H., Lerner, B.M., Lopez-Hilifiker, F., Mao, J., Marvin, M.R., Peischl, J., Pollack, I.B., Roberts, J.M., Ryerson, T.B., Thornton, J.A., Veres, P.R., Warneke, C., 2016. Formaldehyde production from isoprene oxidation across NOx regimes. Atmos. Chem. Phys. 16, 2597–2610.

Wu, X., Li, M., Chen, J., Wang, H., Xu, L., Hong, Y., Zhao, G., Hu, B., Zhang, Y., Dan, Y., Yu, S., 2020. The characteristics of air pollution induced by the quasi-stationary front: formation processes and influencing factors. Sci. Total Environ. 707, 136194.

Wu, X., Xu, L., Hong, Y., Chen, J., Qiu, Y., Hu, B., Hong, Z., Zhang, Y., Liu, T., Chen, Y., Bian, Y., Zhao, G., Chen, J., Li, M., 2019. The air pollution governed by subtropical high in a coastal city in Southeast China: formation processes and influencing mechanisms. Sci. Total Environ. 692, 1135–1145.

Xia, M., Wang, T., Wang, Z., Chen, Y., Peng, X., Huo, Y., Wang, W., Yuan, Q., Jiang, Y., Guo, H., Lau, C., Leung, K., Yu, A., Lee, S., 2022. Pollution-derived Br2 boosts oxidation power of the coastal atmosphere. Environ. Sci. Technol. 56 (17), 12055–12065.

Xue, L.K., Gu, R.R., Wang, T., Wang, X.F., Saunders, S., Blake, D., Louie, P.K.K., Luk, C.W.Y., Simpson, I., Xu, Z., Wang, Z., Gao, Y., Lee, S.C., Mellouki, A., Wang, W.X., 2016. Oxidative capacity and radical chemistry in the polluted atmosphere of Hong Kong and Pearl River Delta region: analysis of a severe photochemical smog episode. Atmos. Chem. Phys. 16, 9891–9903.

Yang, X., Xue, L., Wang, T., Wang, X., Gao, J., Lee, S., Blake, D.R., Chai, F., Wang, W., 2018. Observations and explicit modeling of summertime carbonyl formation in Beijing: identification of key precursor species and their impact on atmospheric oxidation chemistry. J. Geophys. Res. Atmos. 123, 1426–1440.

Yang, X., Zhang, G., Sun, Y., Zhu, L., Wei, X., Li, Z., Zhong, X., 2020. Explicit modeling of background HCHO formation in southern China. Atmos. Res. 240, 104941.

Yang, Y., Shao, M., Keßel, S., Li, Y., Lu, K., Lu, S., Williams, J., Zhang, Y., Zeng, L., Nölscher, A.C., Wu, Y., Wang, X., Zheng, J., 2017. How the OH reactivity affects the ozone production efficiency: case studies in Beijing and Heshan,China. Atmos. Chem. Phys. 17, 7127–7142.

Yang, Y., Shao, M., Wang, X., Nölscher, A.C., Kessel, S., Guenther, A., Williams, J., 2016. Towards a quantitative understanding of total OH reactivity: a review. Atmos. Environ. 134, 147–161.

Yang, Z., Cheng, H.R., Wang, Z.W., Peng, J., Zhu, J.X., Lyu, X.P., Guo, H., 2019. Chemical characteristics of atmospheric carbonyl compounds and source identification of formaldehyde in Wuhan, Central China. Atmos. Res. 228, 95–106.

Yu, S., Mathur, R., Kang, D., Schere, K., Eder, B., Pleim, J., 2006. Performance and diagnostic evaluation of ozone predictions by the Eta-Community Multiscale Air Quality Forecast System during the 2002 New England Air Quality Study. J. Air Waste Manag. Assoc. 56, 1459–1471.

Yuan, B., Hu, W.W., Shao, M., Wang, M., Chen, W.T., Lu, S.H., Zeng, L.M., Hu, M., 2013. VOC emissions, evolutions and contributions to SOA formation at a receptor site in eastern China. Atmos. Chem. Phys. 13, 8815–8832.

Yuan, B., Shao, M., de Gouw, J., Parrish, D.D., Lu, S., Wang, M., Zeng, L., Zhang, Q., Song, Y., Zhang, J., Hu, M., 2012. Volatile organic compounds (VOCs) in urban air: how chemistry affects the interpretation of positive matrix factorization (PMF) analysis. J. Geophys. Res. Atmos. 117 n/a-n/a.

Zeng, P., Lyu, X.P., Guo, H., Cheng, H.R., Wang, Z.W., Liu, X.F., Zhang, W.H., 2019. Spatial variation of sources and photochemistry, of formaldehyde in Wuhan,Central China. Atmos. Environ. 214, 116826.

Zhang, G., Hu, R., Xie, P., Lu, K., Lou, S., Liu, X., Li, X., Wang, F., Wang, Y., Yang, X., Cai, H., Wang, Y., Liu, W., 2022. Intercomparison of OH radical measurement in a complex atmosphere in Chengdu,China. Sci. Total. Environ. 838, 155924.

Zhang, K., Duan, Y., Huo, J., Huang, L., Wang, Y., Fu, Q., Wang, Y., Li, L., 2021a. Formation mechanism of HCHO pollution in the suburban Yangtze River Delta region, China: a box model study and policy implementations. Atmos. Environ. 267, 118755.

Zhang, K., Huang, L., Li, Q., Huo, J., Duan, Y., Wang, Y., Yaluk, E., Wang, Y., Fu, Q., Li, L., 2021b. Explicit modeling of isoprene chemical processing in polluted air masses in suburban areas of the Yangtze River Delta region: radical cycling and formation of ozone and formaldehyde. Atmos. Chem. Phys. 21, 5905–5917.

Zhang, L., Brook, J.R., Vet, R., 2003. A revised parameterization for gaseous dry deposition in air-quality models. Atmos. Chem. Phys. 3, 2067–2082.

Zhang, Y.N., Xue, L.K., Carter, W.P.L., Pei, C.L., Chen, T.S., Mu, J.S., Wang, Y.J., Zhang, Q.Z., Wang, W.X., 2021c. Development of ozone reactivity scales for volatile organic compounds in a Chinese megacity. Atmos. Chem. Phys. 21, 11053–11068.

Zhu, J., Wang, S., Wang, H., Jing, S., Lou, S., Saiz-Lopez, A., Zhou, B., 2020. Observationally constrained modeling of atmospheric oxidation capacity and photochemical reactivity in Shanghai,China. Atmos. Chem. Phys. 20, 1217–1232.

Zhu, L., Jacob, D.J., Keutsch, F.N., Mickley, L.J., Scheffe, R., Strum, M., Gonzalez Abad, G., Chance, K., Yang, K., Rappengluck, B., Millet, D.B., Baasandorj, M., Jaegle, L., Shah, V., 2017. Formaldehyde (HCHO) as a hazardous air pollutant: mapping surface air concentrations from satellite and inferring cancer risks in the United States. Environ. Sci. Technol. 51, 5650–5657.